Journal of Zhejiang University-SCIENCE A 2026 27(4):417-436
www.jzus.zju.edu.cn; www.springer.com/journal/11582
E-mail: jzus_a@zju.edu.cn

Research Article

https://doi.org/10.1631/jzus.A2500135

Check for updates

A simplified analytical model for geosynthetic-reinforced pile-supported embankments with cohesive fills

Xiang-Shen FU[1,2], Ren-Peng CHEN[1,2], Han-Lin WANG[1,2]✉, Xin KANG[1,2], Daniel DIAS[3]

[1]*College of Civil Engineering, Hunan University, Changsha 410082, China*
[2]*International Joint Research Center for Construction and Maintenance of Engineering Structures under Extreme Conditions, Changsha 410082, China*
[3]*Laboratory 3SR, CNRS UMR 5521, Grenoble Alpes University, Grenoble 38000, France*

Abstract: Most current design methods for geosynthetic-reinforced pile-supported (GRPS) embankments neglect the influence of fill cohesion, and are therefore only suitable for cohesionless fills. However, cohesive fills are also widely used in GRPS embankments. To address this issue, we present an analytical model that expands the hemispherical arching model to incorporate cohesive fill properties. The proposed model integrates the soil arching effect, the tensioned membrane effect, and subsoil support to provide a simple approach for analyzing load transfer in GRPS embankments. To evaluate the effectiveness of the proposed model, a comparison with four well-known design methods is conducted using several case studies. This comparison demonstrates that the proposed model shows good agreement with the measured data, validating the reliability and applicability of our method. A parametric study is also performed, with the results indicating that the cohesion of fills enhances load transfer in GRPS embankments, resulting in a greater pile efficacy and a lower geosynthetic deflection. These findings provide valuable insights for the construction of GRPS embankments.

Key words: Geosynthetics; Cohesive fill; Pile-supported embankment; Soil arching effect; Load transfer; Simplified analytical model

1 Introduction

Compared to conventional soil improvement techniques like soil replacement and preloading, the geosynthetic-reinforced pile-supported (GRPS) technique displays better performance in reducing overall and differential settlements, enabling shorter construction periods (van Eekelen and Han, 2020; Chen et al., 2024). Thus, GRPS embankment systems have found extensive applications in railways (Chen et al., 2016; Briançon and Simon, 2017; Wang et al., 2018, 2019a, 2019b; Wang and Chen, 2019; Nguyen et al., 2023), highways (Liu et al., 2007; Chen et al., 2010), and power plants (Xing et al., 2014; Chen et al., 2021). In a GRPS embankment system, the soft subsoil is reinforced using a rigid network of piles in soft subsoil. Above the pile caps, single or multiple layers of geosynthetic reinforcements can be installed. Due to the difference in stiffness between the piles and the surrounding subsoil, differential settlements may occur, causing the embankment fills between piles to move downward. However, this tendency is restrained by the shear resistance generated in the embankment fills. As a result, part of the embankment load is transferred to the pile caps. This is known as the soil arching effect (Terzaghi, 1943). Additionally, the stretching of geosynthetics caused by differential settlements can reduce settlement and enhance load transfer to the piles, which is known as the tensioned membrane effect (Pham, 2020). Therefore, in GRPS embankment systems, a considerable part of the embankment load, together with the surcharge load, is able to be transferred to the piles through the load transfer mechanism (i.e., the soil arching effect and the tensioned membrane effect), as shown in Fig. 1.

The design of GRPS embankments typically begins with evaluating the soil arching effect, as it is

✉ Han-Lin WANG, wanghanlin@hnu.edu.cn
Xiang-Shen FU, https://orcid.org/0000-0003-2095-7005
Han-Lin WANG, https://orcid.org/0000-0002-5416-9392

Received Apr. 18, 2025; Revision accepted Sept. 3, 2025;
Crosschecked Jan. 7, 2026; Online first Mar. 31, 2026

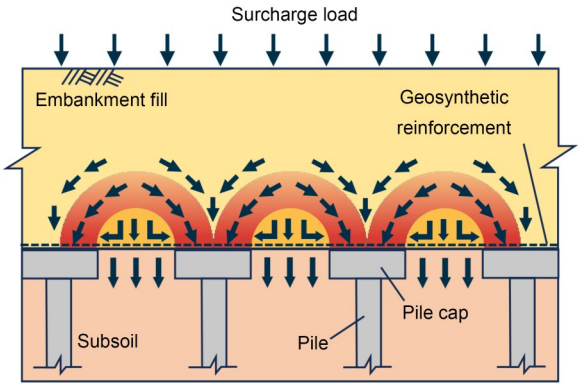

Fig. 1 Illustration of load transfer in GRPS embankment systems

recognized as the primary mechanism for GRPS embankment load transfer (Pham and Dias, 2022). To date, the soil arching effect has been explored by numerous researchers through field tests (Liu et al., 2007, 2015; Chen et al., 2010, 2021; van Eekelen et al., 2020), physical model tests (Hewlett and Randolph, 1988; Low et al., 1994; Fagundes et al., 2017; Rui et al., 2019; Al-Naddaf and Han, 2021; Zhou et al., 2023; Chen et al., 2025a, 2025b; Zhang et al., 2025, 2026), and numerical investigations (Han et al., 2012; Lai et al., 2016; Bao et al., 2020; Pham and Dias, 2021a; Smith et al., 2022; Chen et al., 2023; Fu et al., 2025). In addition, several analytical models have been developed for calculating the soil arching effect. These models can generally be categorized into four groups based on their assumptions: empirical soil arching models (Marston and Anderson, 1913; Jones et al., 1990), rigid soil arching models (Carlsson, 1987; Guido et al., 1987; van Eekelen et al., 2003), frictional soil arching models (Terzaghi, 1943; Handy, 1985; McKelvey, 1994), and limit equilibrium soil arching models (Hewlett and Randolph, 1988; Zaeske, 2001; van Eekelen et al., 2013). Some of these models have been incorporated into existing design codes and technical guidelines. For instance, the hemispherical arching model proposed by Hewlett and Randolph (1988) is integrated into the British Standard BS8006-1 (BSI, 2010); the nonconcentric hemispherical arching model from Zaeske (2001) is utilized in the German Standard EBGEO (German Geotechnical Society, 2011); the concentric hemispherical arching model developed by van Eekelen et al. (2013) is employed in the Dutch Design Guideline (van Eekelen and Brugman, 2016); the wedge-shaped model introduced by Carlsson (1987) is adopted in the Nordic Guideline (Rogbeck et al., 2003). Analysis of these existing models consistently indicates that calculated soil arching effects in GRPS embankments mainly depend on the size and layout of the piles (pile caps), the embankment fill properties (e.g., the unit weight and the internal friction angle), and the embankment height. Meanwhile, the properties of the geosynthetic reinforcement and subsoil also affect the final performance of GRPS embankments.

It is worth noting that most existing analytical models for GRPS embankment design were developed with the assumption of cohesionless fills. Therefore, these models are limited to cohesionless fills, but such fills are frequently used in practice, as demonstrated by numerous studies (Liu et al., 2007, 2015; Chen et al., 2010, 2021; Nunez et al., 2013; Cao et al., 2016; Zhang et al., 2018; Zhao et al., 2019; Lu et al., 2020; Wang and Yin, 2020; Wang et al., 2024; Ye et al., 2024; Fu et al., 2026). Xu et al. (2016) conducted scaled model tests and found that cohesive embankment fills enhance the soil arching effect, increase the pile efficacy (defined as the ratio of the load on the pile cap to the total applied load), and reduce the pile-soil differential settlements compared to cohesionless embankment fills. These findings were corroborated by Pham and Dias (2021a) through 3D numerical analysis. Huckert et al. (2016) observed similar behavior in full-scale tests, highlighting that the collapse mechanisms of cohesive and cohesionless fills are significantly different. Additionally, numerical trapdoor tests by Lai et al. (2020) and Chen et al. (2022) demonstrated that cohesion has a pronounced influence on the soil arching effect in cohesive-frictional materials. Despite these advancements, a comprehensive theoretical approach that effectively incorporates the influence of cohesive fills into GRPS embankment design remains elusive. Pham and Dias (2021b) reviewed case studies and concluded that most existing analytical models are less applicable to cohesive fills than cohesionless fills. Although Pham et al. (2022) introduced an analytical model that accounted for cohesive fills, the ultimate state at the soil arching foot was neglected, increasing the risk of failure, especially when the fill height is relatively high (Hewlett and Randolph, 1988; Low et al., 1994; Zhuang et al., 2014). Furthermore, the high complexity of their model, which involves 14 input parameters, limits its practicality for engineers. On the other hand, disregarding the fill cohesion

entirely, as suggested by some researchers (van Eekelen et al., 2015), could lead to overly conservative designs, particularly when high-cohesion fill materials such as lime-stabilized soil or cement-treated sand are used.

While numerical and field investigations remain essential methods for analyzing GRPS embankments, they often entail high computational demands, significant costs, and lengthy execution times, which limit their practicality for early-stage design or rapid assessments. In contrast, analytical models, which are favored by many researchers (van Eekelen et al., 2013; Zhuang et al., 2014; Lai et al., 2021; Pham and Dias, 2022; Pham et al., 2022; Zhang et al., 2022; Nguyen et al., 2023; Zhou et al., 2023), can offer computational efficiency and clear theoretical insights into key mechanisms, guiding the interpretation of numerical and field results.

In this study, a simplified analytical model is developed that explicitly considers the influence of cohesive fills on load transfer in GRPS embankments. As an extension of the typical hemispherical arching model, soil elements at both the crown and soil arching foot are considered during the calculation of the soil arching effect in GRPS embankments. Additionally, the load-carrying contributions of the geosynthetic reinforcement and subsoil are incorporated into the proposed model. Simplified assumptions are adopted to ensure practicality while maintaining theoretical accuracy. The main novelty of the proposed model lies in its ability to account for cohesive fill properties, which are overlooked in most existing methods, and its accessibility and efficiency as a design tool for engineers. The feasibility and applicability of the proposed model are demonstrated through comparisons with several existing design methods on experimental data. Furthermore, a parametric study is performed to enhance understanding of the input parameters influencing embankment behavior.

2 Analysis of GRPS embankments

The following assumptions are adopted in the development of our analytical model: (1) the embankment fill and soft subsoil are homogeneous and isotropic, and only vertical deformations are considered; (2) the piles are considered rigid, while the friction between piles and surrounding subsoils is neglected; (3) the ratio of the embankment height to the center-to-center spacing between piles in the diagonal direction is greater than 0.5; (4) the creep of the geosynthetic reinforcement and the subsoil is not considered. These assumptions were also adopted in several current analytical solutions (BSI, 2010; German Geotechnical Society, 2011; Zhuang et al., 2014; van Eekelen and Brugman, 2016; Lai et al., 2021; Pham and Dias, 2022; Zhang et al., 2022) to achieve simplicity and practicality.

2.1 Analysis of the soil arching effect

2.1.1 Hemispherical arching model (Hewlett and Randolph, 1988)

Limit equilibrium models are commonly utilized in current design codes (or guidelines) for GRPS embankments, allowing for the consideration of load distribution shape (Low et al., 1994; Rogbeck et al., 2003; BSI, 2010; German Geotechnical Society, 2011; van Eekelen and Brugman, 2016). The hemispherical arching model proposed by Hewlett and Randolph (1988) is one of the most widely used soil arching models based on limit equilibrium theory. This model involves a series of hemispherical domes, as shown in Fig. 2. It offers a clear analytical framework for the soil arching effect without imposing excessive computational demands. Therefore, we select it as the foundational framework for our analysis of the soil arching effect in cohesive embankment fills.

2.1.2 Failure at the crown of arching

The stress analysis of the crown of arching is shown in Fig. 2b. The stress equilibrium in the vertical direction must follow:

$$\frac{\mathrm{d}\sigma_r}{\mathrm{d}r}+\frac{2(\sigma_r-\sigma_\theta)}{r}=-\gamma, \tag{1}$$

where σ_r and σ_θ represent the radial and tangential stresses, respectively (kPa); r represents the hemisphere radius (m); γ represents the average unit weight of the embankment fills (kN/m^3).

At the limit state, considering the embankment fills' cohesion contribution to the shear strength, the tangential stress σ_θ can be expressed as:

$$\sigma_\theta=K_\mathrm{p}\sigma_r+2c\chi\sqrt{K_\mathrm{p}}, \tag{2}$$

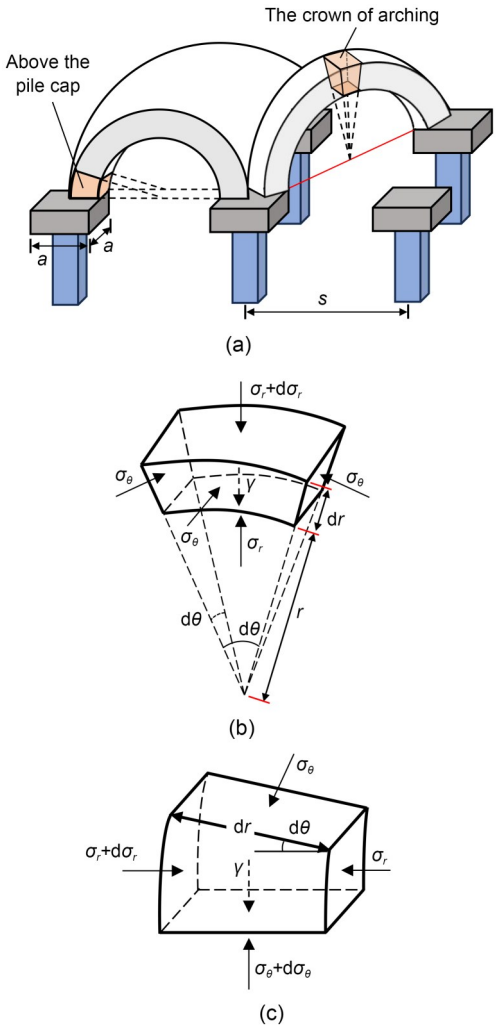

Fig. 2 Hemispherical arching model of Hewlett and Randolph (1988): (a) conceptual representation; (b) stress analysis of soil element at the crown of arching; (c) stress analysis of soil element above the pile cap. The parameters are explained in the maintext

$$\chi=\frac{\gamma H\tan\varphi+c}{10(\gamma H\tan\varphi)}, \tag{3}$$

where K_p represents the passive earth pressure Rankine coefficient, $K_p=\tan^2(45°+\varphi/2)$; φ is the internal embankment fill friction angle (°); c is the embankment fill cohesion (kPa); H is the equivalent embankment height (m), $H=(\gamma h+q)/\gamma$; h represents the actual embankment height (m); q denotes the surcharge load (kPa). In particular, χ is a dimensionless cohesion coefficient that integrates the cohesion contribution with the shear strength, accounting for the unit weight, the embankment height, and the soil internal friction angle.

As detailed in Eq. (3), the numerator ($\gamma H\tan\varphi+c$) provides shear strength considering the cohesion, and is then divided by a shear strength without cohesion ($\gamma H\tan\varphi$), making the result a dimensionless quantity. The introduction of γH allows the influence of soil height on the cohesion to be considered. Further dividing the result by 10 is an empirical scaling approach, which was also adopted by Pham et al. (2022), to ensure that the cohesion coefficient χ falls within a range typical for soil conditions and embankment heights in engineering practice (generally less than 1). This avoids unrealistically high cohesion contributions to the shear strength at the limit state, thereby improving the stability and applicability of the model across various soil conditions. The dimensionless cohesion coefficient χ can adjust the cohesion contribution to the shear strength at the limit state according to the soil properties (e.g., cohesion, internal friction angle, and unit weight). Additionally, it allows the cohesion's influence on the shear strength to vary with the soil height. This plays an essential role in improving the accuracy and applicability of our proposed model.

By substituting Eq. (2) into Eq. (1), and applying the boundary condition at the top of the crown, where $r=s/\sqrt{2}$, $\sigma_r=\gamma\left(H-s/\sqrt{2}\right)$, the radial stress σ_r at any radius within the arching can be determined as:

$$\sigma_r=\gamma\left[H-\left(s/\sqrt{2}\right)\left(\frac{2K_p-2}{2K_p-3}\right)\right]\left(\frac{\sqrt{2}\,r}{s}\right)^{2K_p-2}+\frac{\gamma r}{2K_p-3}+\left[1-\left(\frac{\sqrt{2}\,r}{s}\right)^{2K_p-2}\right]A, \tag{4}$$

where s represents the center-to-center pile spacing (m).

A is a parameter which is defined as:

$$A=\frac{2c\chi\sqrt{K_p}}{1-K_p}. \tag{5}$$

Note that a square arrangement of piles is assumed in this study.

Obviously, the inner boundary radius of the crown top is $(s-a)/\sqrt{2}$ (a is the width of the square pile caps (m)). Therefore, the radial (vertical) stress at this inner boundary can be obtained by substituting $r=$

$(s-a)/\sqrt{2}$ into Eq. (4). Adding this to the vertical stress $\gamma(s-a)/\sqrt{2}$ caused by the embankment fills beneath the arching, the vertical stress acting on the embankment base σ_v can be derived as:

$$\sigma_v=\sigma_r\Big|_{r=(s-a)/\sqrt{2}}+\gamma(s-a)/\sqrt{2}. \tag{6}$$

Next, combining Eqs. (4) and (6), the vertical stress acting on the base of the embankment can be determined as:

$$\begin{aligned}\sigma_v=\gamma\left[H-(s/\sqrt{2})\left(\frac{2K_p-2}{2K_p-3}\right)\right]\left(1-\frac{a}{s}\right)^{2K_p-2}+\\ \frac{s-a}{\sqrt{2}}\frac{2K_p-2}{2K_p-3}\gamma+\left[1-\left(1-\frac{a}{s}\right)^{2K_p-2}\right]A.\end{aligned} \tag{7}$$

For a circular pile cap, the equivalent width can be calculated as $a=d\sqrt{\pi}/2$, where d represents the circular pile cap diameter (m).

The vertical stress σ_v is assumed to act uniformly across the embankment base. This vertical stress is also regarded as the total residual stress borne by the geosynthetic reinforcement and the subsoil. Within the contributed region per pile (cap), the overall vertical equilibrium condition requires that:

$$s^2\gamma H=(s^2-a^2)\sigma_v+P_c^a, \tag{8}$$

where P_c^a is the portion of loading distributed to the pile cap by the soil arching effect (kN). Accordingly, the pile efficacy resulting from the soil arching effect (E_a), which represents the percentage of the total load (including the surcharge) distributed directly onto the pile caps by the soil arching effect, can be determined as:

$$E_a=\frac{P_c^a}{s^2\gamma H}=1-\frac{(s^2-a^2)\sigma_v}{s^2\gamma H}. \tag{9}$$

2.1.3 Failure at the arching foot

The pile caps are considered to be at the bases of four plane-strain arching feet, as shown in Fig. 2a. For each one, the stress analysis above the pile cap is detailed in Fig. 2c. Stress equilibrium in the horizontal direction requires that:

$$\frac{d\sigma_r}{dr}+\frac{\sigma_r-\sigma_\theta}{r}=0. \tag{10}$$

At the limit state, the relationship between the tangential stress σ_θ and the radial stress σ_r also satisfies Eq. (2). In addition, the radial stress on the inner boundary at the base of a plane-strain arching foot, with a radius of $r=(s-a)/2$, can be determined as:

$$\sigma_r=K_p\sigma_v+2c\chi\sqrt{K_p}. \tag{11}$$

Substituting Eq. (2) into Eq. (10), and using the boundary conditions of $r=(s-a)/2$ and $\sigma_r=K_p\sigma_v+2c\chi\sqrt{K_p}$, the radial stress σ_r at any radius within the arching foot can be calculated as:

$$\sigma_r=K_p(\sigma_v-A)\left(\frac{2r}{s-a}\right)^{K_p-1}+A. \tag{12}$$

Under this condition, the portion of loading distributed to the pile cap by the soil arching effect (P_c^a) can be calculated by integrating the tangential stress σ_θ across the pile cap:

$$P_c^a=4\int_{(s-a)/2}^{s/2}\sigma_\theta(s-2r)dr. \tag{13}$$

Combining Eqs. (2), (12), and (13), P_c^a can be obtained as:

$$\begin{aligned}P_c^a=2(s-a)\frac{K_p}{K_p+1}\left[s\left(1-\frac{a}{s}\right)^{-K_p}-s-K_pa\right]\\ (\sigma_v-A)+Aa^2=B(\sigma_v-A)+Aa^2,\end{aligned} \tag{14}$$

where B is a parameter defined as:

$$B=2(s-a)\frac{K_p}{K_p+1}\left[s\left(1-\frac{a}{s}\right)^{-K_p}-s-K_pa\right]. \tag{15}$$

By replacing Eq. (8) with Eq. (14), the solution for σ_v can be calculated as:

$$\sigma_v=\frac{s^2\gamma H-A(a^2-B)}{(s^2-a^2)+B}. \tag{16}$$

Thus, the pile efficacy component E_a by the soil arching effect is:

$$E_a = \frac{P_c^a}{s^2\gamma H} = \frac{B(\sigma_v - A) + Aa^2}{s^2\gamma H}. \tag{17}$$

In Eqs. (4)–(17), the terms containing the parameter A essentially represent the main novelty of the proposed model, accounting for the effect of fill cohesion on the soil arching effect from a theoretical perspective. Importantly, when the cohesion parameter is set to zero (i.e., A=0 in Eqs. (7) and (16)), the soil arching component of the proposed model becomes mathematically identical to the original hemispherical arching model proposed by Hewlett and Randolph (1988). This ensures that our approach still exactly reproduces the original hemispherical arching model for cohesionless soils, while extending its applicability to cohesive GRPS embankments.

It should be noted that the cohesion parameter in this study represents the short-term undrained shear strength of the fill material, which is applicable to the immediate post-construction stage, when undrained conditions dominate. For long-term service conditions, in which consolidation reduces the effective cohesion, the cohesion term should be reduced or omitted, and the drained shear strength parameters are adopted in the model.

2.2 Deflection behavior of the geosynthetic reinforcement

Under the embankment's weight and surcharge, the subsoil settles, causing a deflection of the geosynthetic reinforcement. This deflected shape enables the geosynthetic to transfer part of the applied load to the pile caps, reducing the load on the subsoil; this is known as the tensioned membrane effect (Han and Gabr, 2002; Pham, 2020; Ye et al., 2020; Sun et al., 2025). Numerical results from Pham and Dias (2021a) suggested that the deformation of geosynthetic closely follows a circular shape in GRPS embankments. Notably, other deformation shapes have been proposed in the literature, such as the parabolic shape suggested by Zaeske (2001) and the third-order power-law shape presented by van Eekelen et al. (2012). In this study, the circular deformation model is adopted for its simplicity, as illustrated in Fig. 3.

The average geosynthetic strain due to stretching can be represented in relation to the maximum deflection as:

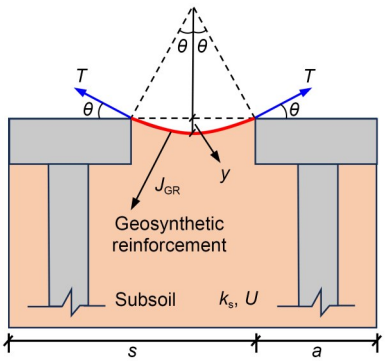

Fig. 3 Deformation analysis of the geosynthetic reinforcement between adjacent piles. The parameters are explained in the maintext

$$\varepsilon = \frac{8}{3}\left(\frac{y}{s-a}\right)^2, \tag{18}$$

where ε is the average axial strain of the geosynthetic reinforcement and y represents the maximum deflection of the geosynthetic reinforcement at the mid-span between piles (m). Assuming a linear elastic response of the geosynthetic reinforcement, the geosynthetic tension induced by vertical stress can be determined as:

$$T = \varepsilon J_{GR}, \tag{19}$$

where T represents the geosynthetic tension (kN/m) and J_{GR} denotes the geosynthetic tensile stiffness (kN/m).

On the other hand, the geosynthetic tension T can be estimated through tensioned membrane theory for a circular deformation model (Low et al., 1994):

$$T = \sigma_{GR}\Omega(s-a), \tag{20}$$

where σ_{GR} represents the vertical stress borne by the geosynthetic reinforcement (kPa), and Ω is a dimensionless factor that is defined as:

$$\Omega = \frac{1}{4}\left(\frac{2y}{s-a} + \frac{s-a}{2y}\right). \tag{21}$$

Combining Eqs. (18)–(21), the vertical stress borne by the geosynthetic reinforcement σ_{GR} can be expressed as:

$$\sigma_{GR} = \frac{64y^3 J_{GR}}{3(s-a)^2\left[4y^2 + (s-a)^2\right]}. \tag{22}$$

2.3 Subsoil reaction

Subsoil support in GRPS embankments has been reported in several studies (Zhuang et al., 2014; Zhuang and Wang, 2016; Pham, 2020; van Eekelen and Han, 2020). The comparisons conducted by Pham and Dias (2021b) demonstrated that the analytical methods considering subsoil support, e.g., van Eekelen and Brugman (2016) and German Geotechnical Society (2011), yield better predictions of the measured data than the methods without subsoil support consideration, such as BSI (2010). Hence, subsoil support is considered in the present model.

To simplify the analysis, a linear subsoil model is used, similar to Winkler's model. Note that in GRPS embankments, the maximum subsoil settlement is typically assumed to be equal to the maximum geosynthetic deflection by default (Zhuang et al., 2014; Pham, 2020; Pham and Dias, 2022). Consequently, the reaction pressure induced by the subsoil settlement can be estimated by a linear subsoil model as:

$$\sigma_s = \frac{yk_s}{U}, \tag{23}$$

where σ_s is the upward reaction pressure from the subsoil (kPa); k_s denotes the subsoil reaction modulus (kPa/m or kN/m^3); U is the average subsoil consolidation degree calculated based on Terzaghi's 1D consolidation theory (Terzaghi, 1943).

In Eq. (23), the value of the subsoil reaction modulus k_s is:

$$k_s = E_s / D_{act}, \tag{24}$$

where D_{act} represents the soft subsoil active depth (m) and E_s is the average 1D subsoil deformation modulus at the active depth (kPa). Following Terzaghi et al. (1996), the active depth D_{act} is defined as the soft subsoil depth where the additional stress induced by the applied load is less than 20% of the vertical geostatic stress. For simplification, the empirical equations proposed by Pham (2019) are adopted herein for calculating D_{act} as follows.

For a clayey subsoil,

$$D_{act} = 10 \times \sqrt[4]{\frac{s-a}{6}}, \tag{25a}$$

and for a sandy subsoil,

$$D_{act} = 10 \times \sqrt[4]{\frac{s-a}{30}}. \tag{25b}$$

For an average 1D deformation modulus value of the subsoil E_s, it can be optimally determined through field or laboratory experiments, such as plate load tests and consolidation tests. Note that in the case of soft subsoil multilayers, the equivalent subsoil modulus is:

$$E_s = \frac{\sum E_{si} D_i}{\sum D_i}, \tag{26}$$

where D_i represents the thickness of each layer within the active depth (m) and E_{si} is the corresponding 1D deformation modulus of each layer of subsoil (kPa).

2.4 Closed-form solution

Currently, the maximum geosynthetic deflection y in Eqs. (22) and (23) is an unknown variable. To solve this problem, a stress analysis of the element below the geosynthetic between the pile caps is performed, as shown in Fig. 4. The simple vertical equilibrium can be obtained as:

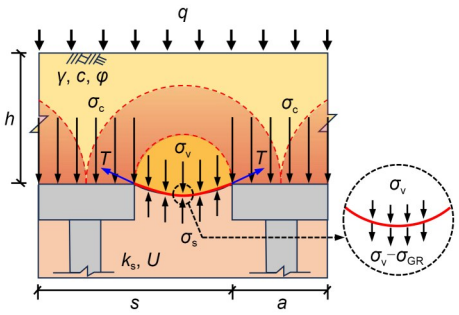

Fig. 4 Stress analysis for the element below the geosynthetic between the pile caps

$$\sigma_v - \sigma_{GR} = \sigma_s. \tag{27}$$

Eq. (27) means that the residual stress induced by the soil arching effect (σ_v) is supported by both the geosynthetic reinforcement (σ_{GR}) and the subsoil (σ_s). By substituting Eqs. (22) and (23) into Eq. (27), the maximum geosynthetic deflection y can be expressed as a reduced cubic equation:

$$\beta_1 y^3 + \beta_2 y^2 + \beta_3 y + \beta_4 = 0, \tag{28}$$

in which

$$\beta_1=64J_{GR}+12(s-a)^2\frac{k_s}{U},\ \beta_2=-12(s-a)^2\sigma_v,$$
$$\beta_3=3(s-a)^4\frac{k_s}{U},\ \beta_4=-3(s-a)^4\sigma_v.$$

Note that in these equations, the value of σ_v is determined by the larger result among those calculated by Eqs. (7) and (16). The value of k_s is estimated by Eq. (24).

By solving Eq. (28), the maximum geosynthetic deflection y is determined. Then, the other unknowns can be calculated by substituting the value of y back into the corresponding equations, such as the geosynthetic tension T using Eqs. (18) and (19), the vertical stress borne by the geosynthetic reinforcement σ_{GR} using Eq. (22), and the subsoil reaction pressure σ_s using Eq. (23).

In addition, utilizing the vertical force equilibrium at the pile cap top, the vertical load transferred onto the pile cap by the tensioned membrane effect can be calculated as:

$$P_c^m=8aT\sin\theta, \tag{29}$$

where P_c^m represents the vertical load transferred onto the pile cap by the tensioned membrane effect (kN) and θ is the deflected angle (°), as shown in Fig. 3. Considering the circular deformation pattern of the geosynthetic reinforcement, a classical approximation for the deflected angle (θ) can be made (Low et al., 1994):

$$\sin\theta=\frac{4[y/(s-a)]}{1+4[y/(s-a)]^2}. \tag{30}$$

By replacing Eq. (29) with Eq. (30), P_c^m can be expressed as:

$$P_c^m=\frac{32aTy(s-a)}{4y^2+(s-a)^2}. \tag{31}$$

The pile efficacy component induced by the tensioned membrane effect (E_m) is thus equal to:

$$E_m=\frac{P_c^m}{s^2\gamma H}. \tag{32}$$

The total pile efficacy (E), which is defined as the ratio of the total load transmitted on the pile cap to the total embankment load including the surcharge, can be written as:

$$E=E_a+E_m. \tag{33}$$

Note that the value of E_a is determined by the lower result of Eqs. (9) and (17).

The stress reduction ratio (η), defined as the ratio of the average vertical stress on the subsoil surface to the average weight of the embankment and surcharge (jointly influenced by soil arching effect and tensioned membrane effect), is calculated as:

$$\eta=\frac{\sigma_s}{\gamma H}. \tag{34}$$

Based on the pile efficacy and the stress reduction ratio, the load transfer mechanism in GRPS embankments can be assessed. Following this, a design flowchart for GRPS embankments using the proposed model is illustrated in Fig. S1 of the electronic supplementary materials (ESM). The proposed model follows a two-step process: First, the load distribution between the pile caps and geosynthetic–subsoil system is evaluated based on the developed soil arching model, which incorporates the influence of fill cohesion. Second, tensioned membrane theory, incorporating subsoil support, is introduced to analyze the load-deflection behavior of the geosynthetic reinforcement. The maximum tensile force/strain of the reinforcement is then calculated accordingly.

3 Validation of the analytical model

To validate the proposed analytical model, a comparison is conducted between our model and existing analytical models across several experimental cases. The other models consist of four widely used design standards: the Nordic design guideline (NGG) (Rogbeck et al., 2003), the British Standard BS8006-1 (BSI, 2010), the German Standard EBGEO (German Geotechnical Society, 2011), and the Dutch Design Guideline (CUR226) (van Eekelen and Brugman, 2016). These analytical models are illustrated in Section S5 of the ESM. The comparison results are

presented in terms of pile efficacy, the maximum deflection of the geosynthetic, and the geosynthetic tension.

3.1 Full-scale field test in Shanghai (Liu et al., 2007)

The monitoring results of a GRPS highway embankment located in a northern suburb of Shanghai, China, were presented by Liu et al. (2007). For clarity, a detailed description of this case is provided in Section S1 of the ESM, and the input parameters for the analytical models are also summarized in Table S1 of the ESM. Table 1 presents a comparison of the results from different analytical models and measurements. Overall, the proposed model shows good agreement with the measured data as compared to the other methods. Although the CUR226 method predicts the total pile efficacy reasonably well, it considerably overestimates the maximum geosynthetic deflection. The other methods display notable deviations from the measured data in terms of the total pile efficacy, maximum geosynthetic deflection, and geosynthetic tension. Notably, despite accounting for subsoil support, the EBGEO method considerably overestimates the geosynthetic deformation in this case. This discrepancy is probably caused by the small value of the improvement area ratio ζ (only equal to 8.7% in this case), which represents the percentage of the total foundation area that the pile caps cover.

3.2 Full-scale field test in Zhejiang (Liu et al., 2015)

Liu et al. (2015) reported a case study on a GRPS embankment for a highway construction project over soft ground in Ningbo, China. A detailed description of this case is available in Section S2 of the ESM, and the corresponding input parameters is also shown in Table S2 of the ESM. Table 2 presents a comparison between the results obtained from the analytical models and the measured data. The proposed model achieves solid agreement with the measurements of the total pile efficacy, maximum deflection, and geosynthetic tension. While the CUR226 method provides a reasonable estimate of the overall pile efficacy, it exaggerates the maximum geosynthetic deflection, as well as the associated tensile forces. The other methods also substantially overpredict these parameters. Compared to the BS8006-1 method (which uses the original hemispherical arching model), the proposed model demonstrates better consistency with the measurements. These results indicate that considering the fill cohesion and the subsoil support yields higher accuracy in estimating the considered parameters of GRPS embankments.

3.3 Full-scale field test in Zhejiang (Chen et al., 2021)

Chen et al. (2021) described a series of field tests for a GRPS embankment on a soft marine deposit located on the coast of the East China Sea. A detailed description of this case is provided in Section S3 of

Table 1 Comparison of calculated and measured results for case of Liu et al. (2007)

Model	E_a (%)	E (%)	η	T (kN/m)	y (mm)
Proposed model	54.8	55.1	0.49	2.9	65.0
CUR226 (van Eekelen and Brugman, 2016)	53.1	57.3	0.46	27.1	107.0
EBGEO (German Geotechnical Society, 2011)	46.2	65.5	0.38	67.0	203.1
BS8006-1 (BSI, 2010)	54.0	100	0	244.0	599.0
NGG (Rogbeck et al., 2003)	51.9	N/A	N/A	128.8	435.1
Measured data	N/A	56.6	0.48	(3.5)	72.0

Parenthesized value is derived by the deflection of geosynthetic and N/A indicates that data were not available

Table 2 Comparison of calculated and measured results for case of Liu et al. (2015)

Model	E_a (%)	E (%)	η	T (kN/m)	y (mm)
Proposed model	73.4	76.1	0.29	5.8	43.4
CUR226 (van Eekelen and Brugman, 2016)	68.8	75.4	0.30	27.2	64.4
EBGEO (German Geotechnical Society, 2011)	62.9	95.5	0.05	59.6	124.5
BS8006-1 (BSI, 2010)	71.4	100	0	107.5	187.4
NGG (Rogbeck et al., 2003)	76.8	N/A	N/A	72.9	154.4
Measured data	N/A	77.7	0.27	(5.0)	40.5

The notations are consistent with those in Table 1

the ESM, and the corresponding input parameters can be found in Table S3 of the ESM. A comparison between the results obtained from different analytical models and field measurements is provided in Table 3. Notably, the proposed model shows superior agreement with the measured data for both the pile efficacy component from soil arching (E_a) and the maximum geosynthetic deflection (y), as compared to the other methods. The CUR226, EBGEO, and NGG methods all slightly overpredict E_a. In addition, the E_a value predicted by the proposed model is close to that given by the BS8006-1 method. This is mainly because the fill cohesion in this project is quite low (5 kPa) while the internal friction angle is relatively high (39°), which limits the influence of cohesion on the soil arching effect. Moreover, it is obvious that the BS8006-1 and NGG methods significantly overestimate the maximum deflection and the geosynthetic tension. This is because subsoil support is not considered in these two methods.

3.4 Full-scale model test (Wang et al., 2019b)

Wang et al. (2019b) constructed a full-scale model of a GRPS railway track-bed, utilizing a concrete slab and a water bag to simulate the pile caps and the surrounding subsoil, respectively. More information about this test is provided in Section S4 of the ESM, and the corresponding input parameter is included in Table S4 of the ESM. The results from various analytical models are compared to the experimental data, as shown in Table 4. The proposed model's predictions match well with the experimental data of pile efficacy, geosynthetic tension, and maximum geosynthetic deflection. The CUR226 and EBGEO methods slightly overpredict E_a, but underpredict y. In contrast, the BS8006-1 and NGG methods still overestimate y, primarily because of the neglect of subsoil support. Note that the cohesion of embankment fills is relatively high (16.3 kPa). As a result, the cohesion effect's enhancement of the soil arching is considerable. Therefore, the proposed model yields a higher value than the BS8006-1 method in terms of E_a. By taking the cohesion effect and subsoil support into account, the predictive accuracy for pile efficacy and geosynthetic deformation is thus improved. This improvement highlights the practical benefits of incorporating cohesive fill effects and subsoil support into analytical frameworks.

3.5 Comprehensive comparison

To assess the reliability and applicability of the proposed model across a broader range of conditions, additional data on pile efficacy and maximum geosynthetic deflection from van Eekelen et al. (2008, 2010), Chen et al. (2010), and Pham and Dias (2021a) are incorporated, alongside the data from the previous four cases. These datasets cover a wider variety of pile configurations, filling materials, and embankment heights,

Table 3 Comparison of calculated and measured results for case of Chen et al. (2021)

Model	E_a (%)	E (%)	η	T (kN/m)	y (mm)
Proposed model	79.4	80.8	0.30	5.8	30.8
CUR226 (van Eekelen and Brugman, 2016)	88.3	90.4	0.15	9.9	25.8
EBGEO (German Geotechnical Society, 2011)	88.1	93.7	0.10	13.1	53.5
BS8006-1 (BSI, 2010)	78.8	100	0	76.2	90.0
NGG (Rogbeck et al., 2003)	87.3	N/A	N/A	61.7	100.8
Measured data	80.1	81.2	0.29	(4.6)	27.5

The notations are consistent with those in Table 1

Table 4 Comparison of calculated and measured results for case of Wang et al. (2019b)

Model	E_a (%)	E (%)	η	T (kN/m)	y (mm)
Proposed model	87.8	89.4	0.15	4.2	20.3
CUR226 (van Eekelen and Brugman, 2016)	91.6	92.3	0.11	1.3	4.8
EBGEO (German Geotechnical Society, 2011)	92.4	92.9	0.10	0.5	13.9
BS8006-1 (BSI, 2010)	83.7	100	0	38.3	61.1
NGG (Rogbeck et al., 2003)	89.4	N/A	N/A	33.7	57.4
Measured data	84.6	87.5	0.18	(4.1)	20.0

The notations are consistent with those in Table 1

enabling a more comprehensive validation. Following the design flowchart shown in Fig. S1 of the ESM and the calculation steps of the different models detailed in Section S5 of the ESM, predictions of pile efficacy and maximum geosynthetic deflection can be obtained. Thereafter, comparisons of different model predictions with measured results for the maximum geosynthetic deflections and the total pile efficacies are illustrated in Figs. 5a and 5b, respectively. Note that the total pile efficacy cannot be calculated by the NGG method. Thus, a model by Pham et al. (2022) is included herein for comparison. It is important to recognize that the actual behavior of the GRPS system is complex, while some simplified assumptions are made in developing equations for each analytical model (e.g., the friction between piles and surrounding subsoils is often ignored to facilitate mathematical modelling). Consequently, these analytical models may find it difficult to achieve perfect agreement with the measured values.

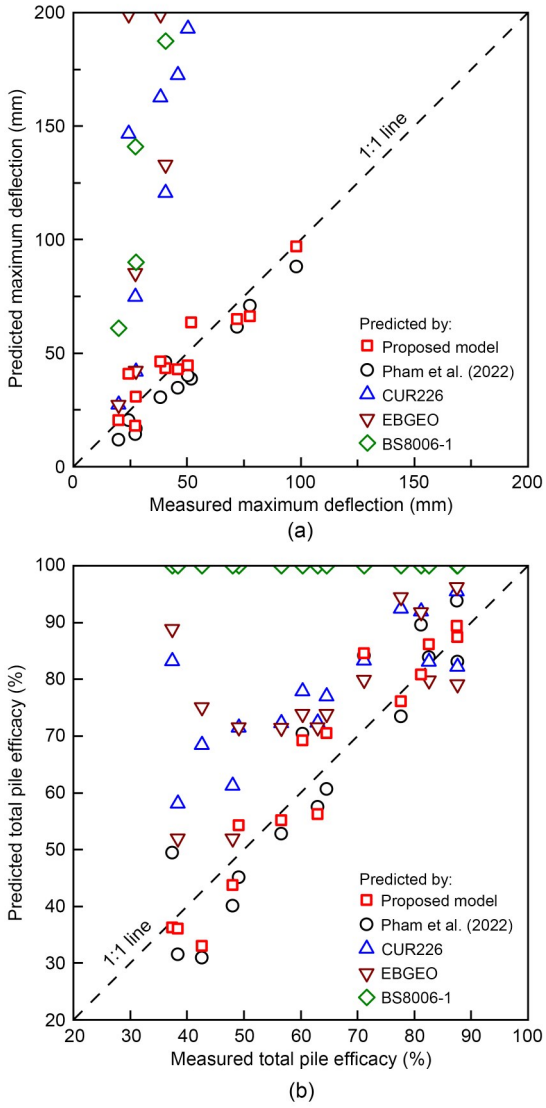

Fig. 5 Comparison of different model predictions against measured results: (a) the maximum geosynthetic deflection and (b) the total pile efficacy

On the whole, the proposed model exhibits a closer match with the measured data than the other methods for both the maximum geosynthetic deflection (Fig. 5a) and the total pile efficacy (Fig. 5b). The BS8006-1 method does not consider subsoil support, instead assuming that the entire embankment load is carried by the piles and geosynthetic reinforcement. Consequently, it significantly overestimates the geosynthetic deflection and produces conservative results, with a total pile efficacy of 100%. Both the CUR226 and EBGEO methods tend to overestimate the geosynthetic deflection, which in turn leads to an overestimation of the total pile efficacy. The EBGEO method includes the subsoil support in the design, but only for the area beneath the reinforcement strips between adjacent piles, which can result in an overestimation of the geosynthetic deflection and tension. Regarding the CUR226 method, the main reason for overestimating the geosynthetic deflection (which results in a slight overestimation of total pile efficacy) might be not considering the degree of subsoil consolidation, which has been indicated as playing an important role in estimating the complex behavior of GRPS embankments (Zhang et al., 2022). On the other hand, the model proposed by Pham et al. (2022) slightly underestimates the geosynthetic deflection. Therefore, it produces a slight underestimation of the total pile efficacy, likely due to the inverse triangular load distribution on the geosynthetic and the assumption of a parabolic geosynthetic deflection shape in the model.

To further evaluate the performance of the proposed model under relatively high fill conditions, Fig. S2 in the ESM compares the predicted pile efficacy by soil arching (E_a) from the proposed model, the model by Pham et al. (2022), and the corresponding measurements for cases with $H/(s-a)>2.0$. The results indicate that the proposed model generally aligns more closely with the measured values than the predictions from the model of Pham et al. (2022). This improvement can mainly be attributed to improved consideration of the ultimate state at the soil arching foot, which becomes increasingly important under higher

fill heights. In addition, the proposed model incorporates the fill cohesion and subsoil support in a more concise analytical form, requiring only nine input parameters while maintaining predictive accuracy.

4 Parametric study

To better understand the complicated behavior of GRPS embankments, a parametric study is conducted. Five key parameters are considered, including the normalized fill height $H/(s-a)$, the improvement area ratio ζ, the internal friction angle of fills φ, the geosynthetic tensile stiffness J_{GR}, and the subsoil reaction modulus k_s. Moreover, the analysis is extended to consider three different values of fill cohesion to emphasize the influence of cohesion on GRPS embankment performance. In this parametric study, only one parameter is modified at a time, while the others are held constant at the baseline values specified by Chen et al. (2021) (see more details in Section 3.3). The basic parameters used in the parametric study are summarized in Table S5 of the ESM. The results are discussed in terms of the total pile efficacy and the maximum deflection of geosynthetic. These results are obtained for the GRPS embankment described by Chen et al. (2021), which is characterized by a relatively high ζ (36%). Note that different trends may be observed for embankments with substantially different configurations.

4.1 Normalized fill height

Fig. 6a shows the influence of the normalized fill height on the total pile efficacy for different fill cohesion values. It can be observed that the pile efficacy increases with $H/(s-a)$. It reaches a limit value at a relatively high value of $H/(s-a)$. This trend is consistent with the experimental results of previous studies (Xu et al., 2016; Wang et al., 2019b). As the embankment fill height increases, a higher shear resistance is mobilized, resulting in a more significant soil arching effect. On the other hand, a plane emerges where the differential settlement reaches zero when the $H/(s-a)$ is large enough, namely the equal settlement plane. The soil shearing above the equal settlement plane is negligible, having less influence on the soil arching effect. As a result, the growth rate of the pile efficacy decreases significantly following the equal settlement

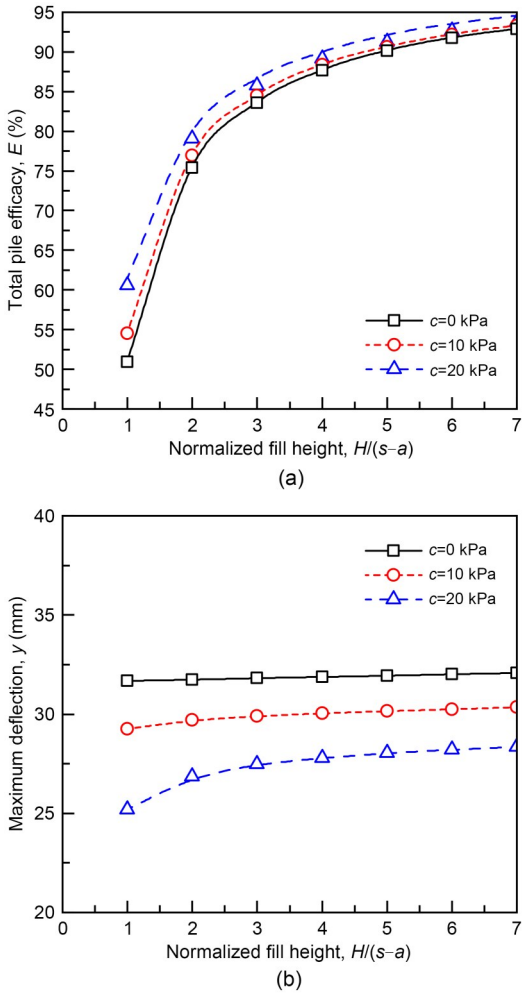

Fig. 6 Influence of normalized fill height on the (a) total pile efficacy and (b) maximum geosynthetic deflection at different cohesion values of fills (note: only the *H* is modified here)

plane formation. This implies that once the normalized fill height exceeds a certain threshold, further increasing the height would not contribute significantly to load transfer improvement, but would potentially increase construction costs. In addition, as shown in Fig. 6a, it seems that the equal settlement plane forms when the normalized fill height $H/(s-a)$ is larger than 2.5, which is termed the critical normalized height. This value can serve as a useful reference in engineering practice, suggesting that embankments with $H/(s-a)$ above 2.5 are unlikely to gain significant additional pile efficacy from further height increases. This agrees well with the results of Zhuang et al. (2012): the pile efficacy increases with the increase of $H/(s-a)$, but tends to approach a limit value when $H/(s-a)$ increases continuously.

From Fig. 6a, one can observe that the pile efficacy increases as the fill cohesion increases. This indicates that the fill cohesion enhances load transfer in GRPS embankments. Nevertheless, as the embankment height increases, the impact of embankment fill cohesion on the pile efficacy becomes less significant. This finding is in keeping with the numerical results reported by Pham and Dias (2021a). According to soil shear strength principles, the shear resistance of soils (τ) comprises both a friction resistance component ($\sigma \tan \varphi$) and a cohesion resistance component (c). A higher embankment corresponds to a higher stress level (σ). As a result, the friction resistance component of fills for mobilizing soil arching is more significant with a higher embankment (reflected in σ_r). This could be the main reason for the cohesion's influence on the pile efficacy when varying the embankment height.

Fig. 6b presents the normalized fill height influence on the maximum geosynthetic deflection for different fill cohesion values. The results show that as the value of $H/(s-a)$ increases, the maximum geosynthetic deflection does not vary significantly, particularly when the cohesion is relatively low. Furthermore, the maximum geosynthetic deflection decreases with increasing fill cohesion. This is because as the fill increases the cohesion, the soil arching effect is enhanced, with less residual stress being carried by the geosynthetic reinforcement and subsoil. Such results further demonstrate the cohesive effect's role in improving load transfer in GRPS embankments.

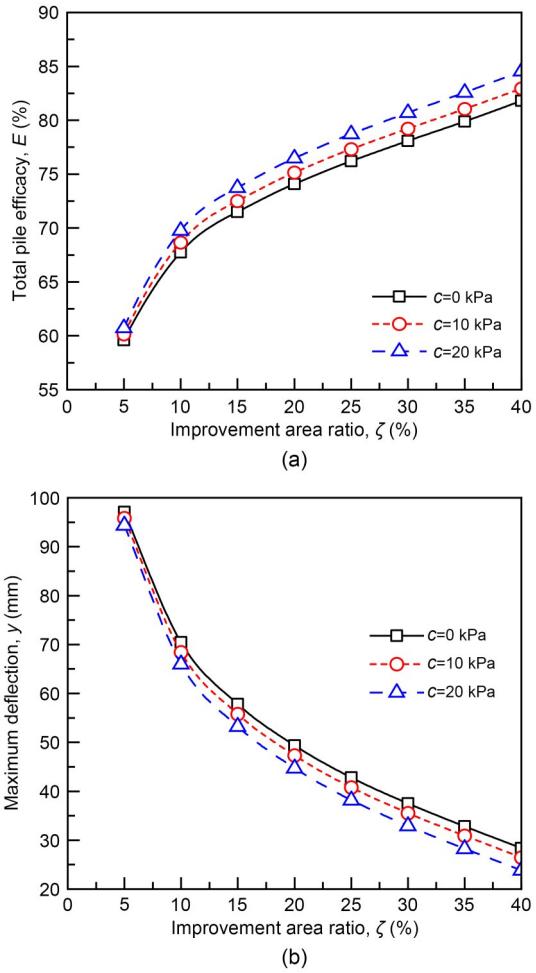

Fig. 7 Influence of improvement area ratio on the (a) total pile efficacy and (b) maximum geosynthetic deflection at different cohesion values of fills

4.2 Improvement area ratio

The improvement area ratio (ζ) represents the percentage of the total foundation area that the pile caps cover, which can be increased by increasing the pile cap width (a) or reducing the pile spacing (s). The former method is adopted herein. Fig. 7 plots the improvement area ratio's effect on the total pile efficacy and maximum geosynthetic deflection. From Fig. 7a, we can see that the pile efficacy increases remarkably with ζ. With ζ increasing, more loads are transferred to the pile cap, leading to a higher pile efficacy. Meanwhile, the pile efficacy shows an increase with the fill cohesion. This means that the cohesive fills strengthen the stress transfer in GRPS embankments, as compared to the case of cohesionless fills. Moreover, note that the cohesion effect becomes more effective when the ζ exceeds approximately 10%. Below this threshold, the contribution of the cohesion to the load transfer is limited. This is because with a lower ζ, the soil arching effect is less stable. As a result, the soil arching that was mobilized due to the friction component is greater than the one mobilized by the cohesion (reflected in σ_v).

As depicted in Fig. 7b, the maximum geosynthetic deflection decreases with the increase of ζ or the cohesion of the fills. Interestingly, the maximum geosynthetic deflection variation trend is opposite to the pile efficacy trend observed in Fig. 7a. Such results agree with expectations, considering that a higher pile efficacy corresponds to a reduced load borne by the geosynthetic. In summary, these results indicate the positive effect of the increase in ζ and cohesion on the load transfer capabilities of GRPS embankments, resulting in greater pile efficacy and less geosynthetic

deflection. Particularly from an engineering perspective, maintaining a ζ above 10% is recommended for cohesive embankments to effectively mobilize the cohesion effect.

4.3 Internal friction angle of fills

Fig. 8a illustrates the influence of internal friction angle of fills on the total pile efficacy for different fill cohesion values. It is observed that the pile efficacy increases with an increase in the internal friction angle and the cohesion, indicating the positive effect of these two parameters on load transfer in GRPS embankments. However, the internal friction angle's influence on the pile efficacy has diminishing returns as it increases further. This tendency is aligned with the numerical results of Pham and Dias (2021a). In addition, the fill cohesion's influence on the pile efficacy is less significant for a relatively high internal friction angle. As mentioned previously, the soil arching mobilization is significantly associated with shear resistance. With the increase of the internal friction angle, the friction resistance component significantly increases, resulting in a lower influence of the cohesion resistance component on the soil arching mobilization (a fact which is reflected in K_p and σ_v). Therefore, the cohesion's influence on the pile efficacy decreases with the increase of the fill's internal friction angle.

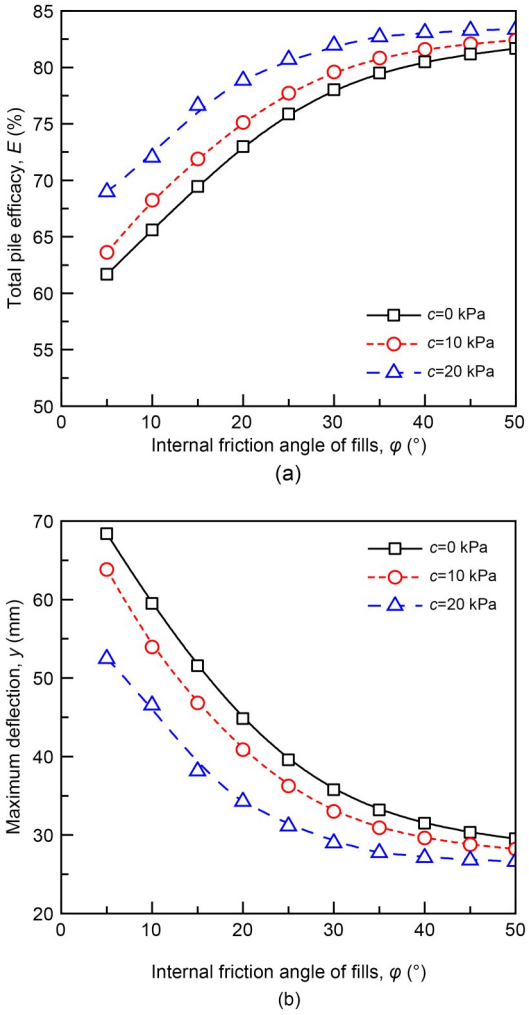

Fig. 8 Influence of internal friction angle of fills on the (a) total pile efficacy and (b) maximum geosynthetic deflection at different cohesion values of fills

Considering that a pile efficacy increase can reduce the loads acting on the geosynthetic, it is reasonable to speculate that the maximum geosynthetic deflection decreases with the increase of the internal friction angle and the cohesion of fills. Indeed, this tendency is observed in our analysis, as presented in Fig. 8b. Similarly, the influence of the internal friction angle and the cohesion of fills on the maximum geosynthetic deflection decreases as the fill internal friction angle increases. All these results indicate that it is efficient to choose fills with a relatively high cohesion and internal friction angle (not exceeding 35° in this analysis) to improve the load transfer in the GRPS embankments.

4.4 Geosynthetic tensile stiffness

Fig. 9a depicts the influence of the geosynthetic tensile stiffness on the total pile efficacy for different fill cohesion values. One can observe that the pile efficacy slightly increases as the geosynthetic tensile stiffness increases. This means that as the geosynthetic tensile stiffness increases, greater embankment loads are transferred to the pile caps. Furthermore, we find that an increase in fill cohesion results in a pile efficacy increase, which indicates the positive effect of the fill cohesion in enhancing the load transfer capabilities of GRPS embankments. However, the cohesion's influence on the pile efficacy is slightly dependent on the geosynthetic tensile stiffness.

The influence of the geosynthetic tensile stiffness on the maximum geosynthetic deflection for different fill cohesion values is presented in Fig. 9b. The results show that as the geosynthetic tensile stiffness increases, the maximum geosynthetic deflection decreases. Note that the geosynthetic tension is associated with both the geosynthetic tensile stiffness and the

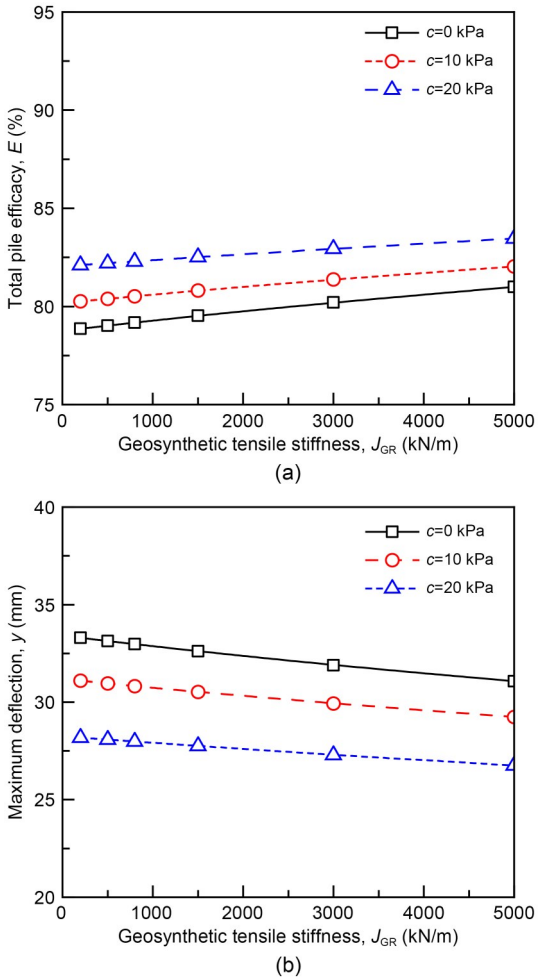

Fig. 9 Influence of geosynthetic tensile stiffness on the (a) total pile efficacy and (b) maximum geosynthetic deflection at different cohesion values of fills

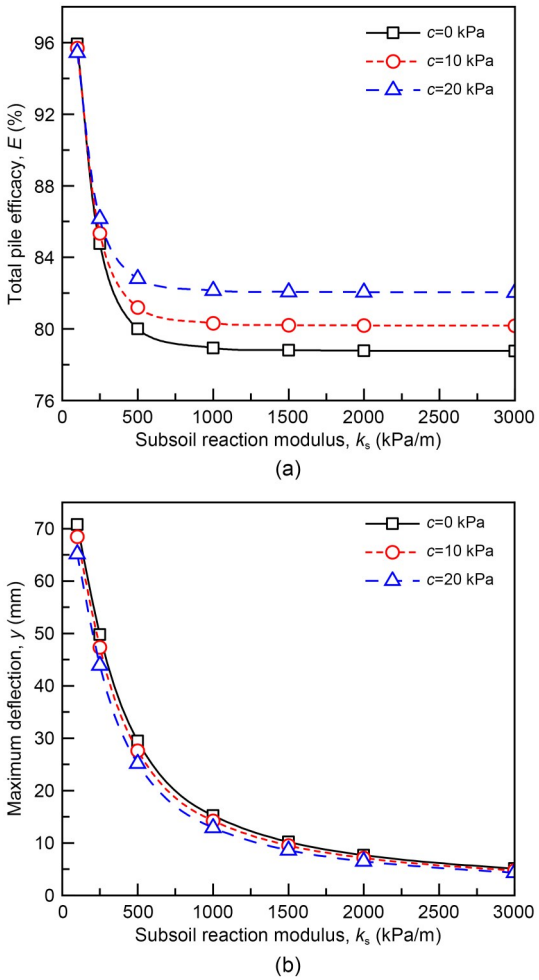

Fig. 10 Influence of subsoil reaction modulus on the (a) total pile efficacy and (b) maximum geosynthetic deflection at different cohesion values of fills

maximum geosynthetic deflection through Eq. (19). This can be considered as the main reason for the insignificant pile efficacy increase as the geosynthetic tensile stiffness increases. In addition, the maximum geosynthetic deflection decreases when the fill cohesion is increased. Consequently, these results showcase the positive influence of the fill cohesion in improving load transfer in GRPS embankments. This suggests that it may be inefficient to enhance load transfer in GRPS embankments by solely increasing the geosynthetic tensile stiffness.

4.5 Subsoil reaction modulus

Fig. 10 presents the variations of the total pile efficacy and the maximum geosynthetic deflection with the subsoil reaction modulus, for different fill cohesion values. As seen in Fig. 10a, the pile efficacy decreases as the subsoil reaction modulus increases, and this pattern follows an exponential function. The pile efficacy approaches a limit value when the subsoil reaction modulus exceeds 500 kPa/m. This means that the subsoil will support greater loads when its reaction modulus is higher (as reflected by σ_s). However, such influence becomes less significant as the subsoil reaction modulus increases. In addition, an increase in the fill cohesion results in a larger pile efficacy. However, for highly compressible subsoils (e.g., when the subsoil reaction modulus is smaller than 500 kPa/m), the pile efficacy depends more strongly on the subsoil reaction modulus than the fill cohesion. This is because for highly compressible subsoils, the geosynthetic deformation is significant and the contribution of the tensioned membrane effect on the pile efficacy becomes considerable. Consequently, when the subsoil

is highly compressible (such as in soft soils), the pile efficacy is more sensitive to variations in the subsoil reaction modulus than to changes in the fill cohesion. In contrast, for incompressible subsoils, all the load between piles is carried directly by the subsoil, so both the soil arching effect and the tensioned membrane effect become negligible.

As shown in Fig. 10b, a nonlinear relationship between the maximum geosynthetic deflection and the subsoil reaction modulus is observed for each case. As the subsoil reaction modulus increases, the maximum geosynthetic deflection decreases sharply. The main reason for this is that with the subsoil reaction modulus increase, more loads are being applied to the subsoil (σ_s), while fewer loads are being borne by the geosynthetic (σ_{GR}). This results in a decrease in the maximum geosynthetic deflection. It also leads to a pile efficacy decrease, as analyzed in Fig. 10a. In addition, an increase in the fill cohesion causes a slight decrease in the maximum geosynthetic deflection. This is because the soil arching effect becomes more significant with the increase in fill cohesion. Thus, fewer residual loads are transferred to the geosynthetic and to the subsoil (reflected in σ_v). On the other hand, with a larger subsoil reaction modulus, more loads are supported by the subsoil, making the fill cohesion's influence on the maximum geosynthetic deflection less significant, as shown in Fig. 10b. These results suggest that the load transfer in the GRPS embankments is particularly sensitive to the subsoil reaction modulus for highly compressible subsoils. Hence, caution should be exercised when evaluating the reaction modulus of highly compressible subsoils.

5 Study limitations

During the development of the model, four assumptions were made. Although satisfactory results were obtained for the proposed model and validated against several engineering cases, there are still limitations that warrant further study. First, only the vertical soil deformations were considered, which may lead to inaccuracies, especially for embankments with large heights or height-to-width ratios, where lateral deformations might be significant. For such cases, more comprehensive methods, such as numerical simulation, may be necessary to achieve higher accuracy. Second, the model assumes homogeneous soil properties, which may not fully represent cases involving heterogeneous soils. Third, the friction between piles and surrounding subsoils is neglected. Hence, caution is required when applying this model to scenarios involving frictional piles or cases where pile-soil interaction plays a dominant role. Moreover, the exclusion of the creep of the geosynthetic reinforcement may result in an underestimation of the geosynthetic deflection. This can be solved by using creep reduction factors for the considered geosynthetics. Additionally, the proposed model is not applicable for relatively low embankments (with a height less than 0.5 times the center-to-center spacing between piles in the diagonal direction), due to the hemispherical arching model utilized. Finally, the scope of the practical case studies is limited by the narrow range of available data. Further validation of the proposed model should therefore consider a broader range of scenarios.

6 Conclusions

In this study, we proposed a simplified analytical model for estimating the load transfer in GRPS embankments, which explicitly incorporated the influence of fill cohesion. The proposed model extends the typical hemispherical arching approach to cohesive soils and also integrates the soil arching effect, tensioned membrane effect, and subsoil support into a unified framework. Our methodology is conceptually and mathematically simple, offering a practical tool for early-stage design and optimization.

The proposed model achieves strong agreement with measured data and generally outperforms four well-known design methods, particularly for cohesive embankments. Neglecting the fill cohesion or subsoil support, as is done in most existing methods, results in overestimation of the maximum geosynthetic deflection and the geosynthetic tension. We found that fill cohesion significantly enhances the load transfer capability of GRPS embankments, resulting in greater pile efficacy and smaller geosynthetic deflection. This effect is more pronounced when the improvement area ratio (ζ) exceeds 10%, and diminishes with increasing normalized fill height or internal friction angle.

It was also revealed that the pile efficacy increases significantly with the normalized height of the

embankment until a critical normalized height (2.5 in this parametric study) is reached, beyond which further increases in fill height yield limited improvements in pile efficacy. Moreover, a higher internal fill friction angle or a higher improvement area ratio both contribute to increased pile efficacy and reduced geosynthetic deflection. For highly compressible subsoils, the load transfer efficiency is highly sensitive to the subsoil reaction modulus. In contrast, for incompressible subsoils, the load between piles is entirely carried by the subsoil, with negligible contributions coming from soil arching or the tensioned membrane effect.

In summary, incorporating fill cohesion is essential for analytical modeling of GRPS embankments under short-term loading conditions. Our proposed model provides a reliable and efficient framework for load transfer analysis in both cohesive and cohesionless GRPS embankments, making it practical for engineering design.

Acknowledgments

This work is supported by the National Key Research and Development Program of China (No. 2025YFE0107200) and the National Natural Science Foundation of China (No. 52378341).

Author contributions

Xiang-Shen FU, Ren-Peng CHEN, and Han-Lin WANG designed the research. Xin KANG and Daniel DIAS processed the corresponding data. Xiang-Shen FU wrote the first draft of the manuscript. Han-Lin WANG helped to organize the manuscript. Xiang-Shen FU and Han-Lin WANG revised and edited the final version.

Conflict of interest

Ren-Peng CHEN is an Editorial Board member of this journal, and is NOT involved in the editorial review or the decision to publish this article. Xiang-Shen FU, Ren-Peng CHEN, Han-Lin WANG, Xin KANG, and Daniel DIAS declare that they have no conflict of interest.

References

Al-Naddaf M, Han J, 2021. Spring-based trapdoor tests investigating soil arching stability in embankment fill under localized surface loading. *Journal of Geotechnical and Geoenvironmental Engineering*, 147(9):04021087. https://doi.org/10.1061/(ASCE)GT.1943-5606.0002601

Bao N, Wei J, Chen JF, et al., 2020. 2D and 3D discrete numerical modelling of soil arching. *Journal of Zhejiang University-SCIENCE A*, 21(5):350-365. https://doi.org/10.1631/jzus.A1900672

Briançon L, Simon B, 2017. Pile-supported embankment over soft soil for a high-speed line. *Geosynthetics International*, 24(3):293-305. https://doi.org/10.1680/jgein.17.00002

BSI (British Standards Institution), 2010. Code of Practice for Strengthened/Reinforced Soils and Other Fills, BS 8006-1: 2010. BSI, London, UK.

Cao WZ, Zheng JJ, Zhang J, et al., 2016. Field test of a geogrid-reinforced and floating pile-supported embankment. *Geosynthetics International*, 23(5):348-361. https://doi.org/10.1680/jgein.16.00002

Carlsson B, 1987. Reinforced Soil, Principles for Calculation. Terratema AB, Linköping, Sweden (in Swedish).

Chen FQ, Luo SC, Lai FW, 2022. New analytical solutions for cohesive-frictional soils above deep active trapdoors. *International Journal of Geomechanics*, 22(12):04022235. https://doi.org/10.1061/(ASCE)GM.1943-5622.0002592

Chen RP, Xu ZZ, Chen YM, et al., 2010. Field tests on pile-supported embankments over soft ground. *Journal of Geotechnical and Geoenvironmental Engineering*, 136(6): 777-785. https://doi.org/10.1061/(ASCE)GT.1943-5606.0000295

Chen RP, Wang YW, Ye XW, et al., 2016. Tensile force of geogrids embedded in pile-supported reinforced embankment: a full-scale experimental study. *Geotextiles and Geomembranes*, 44(2):157-169. https://doi.org/10.1016/j.geotexmem.2015.08.001

Chen RP, Liu QW, Wang HL, et al., 2021. Performance of geosynthetic-reinforced pile-supported embankment on soft marine deposit. *Proceedings of the Institution of Civil Engineers-Geotechnical Engineering*, 174(6):627-644. https://doi.org/10.1680/jgeen.19.00136

Chen RP, Fu XS, Liu QW, et al., 2023. Effect of non-simultaneous movement of adjacent twin-trapdoor on soil arching effect through discrete element method simulation. *Transportation Geotechnics*, 41:101007. https://doi.org/10.1016/j.trgeo.2023.101007

Chen RP, Wang HL, Fu XS, et al., 2024. Upward soil arching effect under unloading: mechanism, theory and engineering application. *Transportation Geotechnics*, 47:101276. https://doi.org/10.1016/j.trgeo.2024.101276

Chen RP, Fu XS, Liu QW, et al., 2025a. Development and validation of deformation-dependent theoretical model for soil arching effect under unloading. *Computers and Geotechnics*, 180:107078. https://doi.org/10.1016/j.compgeo.2025.107078

Chen RP, Xu Y, Wang HL, et al., 2025b. Effect of adjacent excavation on the mechanical response of proximal soil and tunnels in normally consolidated clay: centrifuge model testing and numerical simulation. *Journal of Zhejiang University-SCIENCE A*, 26(10):931-949. https://doi.org/10.1631/jzus.A2500001

Fagundes DF, Almeida MSS, Thorel L, et al., 2017. Load transfer mechanism and deformation of reinforced piled embankments. *Geotextiles and Geomembranes*, 45(2):1-10. https://doi.org/10.1016/j.geotexmem.2016.11.002

Fu XS, Wang HL, Chen RP, et al., 2025. Interaction between adjacent soil-arching effect in homogeneous clay and the corresponding stability analysis of underground voids:

insights from trapdoor modeling. *International Journal of Geomechanics*, 25(8):04025144. https://doi.org/10.1061/IJGNAI.GMENG-9781

Fu XS, Wang HL, Zhai ZJ, et al., 2026. Arching patterns in compacted clay: insights from plane-strain trapdoor tests. *Transportation Geotechnics*, 56:101754. https://doi.org/10.1016/j.trgeo.2025.101754

German Geotechnical Society, 2011. Recommendations for Design and Analysis of Earth Structures Using Geosynthetic Reinforcements–EBGEO. Ernst & Sohn Verlag für Architektur und technische Wissenschaften GmbH & Co. KG, Berlin, Germany. https://doi.org/10.1002/9783433600931

Guido VA, Kneuppel JD, Sweeny MA, 1987. Plate loading tests on geogrid-reinforced earth slabs. Proceedings of Geosynthetics '87 Conference, p.216-225.

Han J, Gabr MA, 2002. Numerical analysis of geosynthetic-reinforced and pile-supported earth platforms over soft soil. *Journal of Geotechnical and Geoenvironmental Engineering*, 128(1):44-53. https://doi.org/10.1061/(ASCE)1090-0241(2002)128:1(44)

Han J, Bhandari A, Wang F, 2012. DEM analysis of stresses and deformations of geogrid-reinforced embankments over piles. *International Journal of Geomechanics*, 12(4):340-350. https://doi.org/10.1061/(ASCE)GM.1943-5622.0000050

Handy RL, 1985. The arch in soil arching. *Journal of Geotechnical Engineering*, 111(3):302-318. https://doi.org/10.1061/(ASCE)0733-9410(1985)111:3(302)

Hewlett WJ, Randolph MF, 1988. Analysis of piled embankments. *Ground Engineering*, 21(3):12-18.

Huckert A, Briançon L, Villard P, et al., 2016. Load transfer mechanisms in geotextile-reinforced embankments overlying voids: experimental and analytical approaches. *Geotextiles and Geomembranes*, 44(3):442-456. https://doi.org/10.1016/j.geotexmem.2015.06.005

Jones CJFP, Lawson CR, Ayres DJ, 1990. Geotextile reinforced piled embankments. *In*: Den Hoedt G (Ed.), Geotextiles, Geomembranes and Related Products. Balkema, Rotterdam, the Netherlands, p.155-160.

Lai FW, Chen SX, Xue JF, et al., 2020. New analytical solutions for shallow cohesive soils overlying trench voids under various slip surfaces. *Transportation Geotechnics*, 25:100411. https://doi.org/10.1016/j.trgeo.2020.100411

Lai HJ, Zheng JJ, Cui MJ, 2021. Improved analytical soil arching model for the design of piled embankments. *International Journal of Geomechanics*, 21(3):04020261. https://doi.org/10.1061/(ASCE)GM.1943-5622.0001929

Lai HJ, Zheng JJ, Zhang RJ, et al., 2016. Visualization of the formation and features of soil arching within a piled embankment by discrete element method simulation. *Journal of Zhejiang University-SCIENCE A*, 17(10):803-817. https://doi.org/10.1631/jzus.A1500302

Liu HL, Ng CWW, Fei K, 2007. Performance of a geogrid-reinforced and pile-supported highway embankment over soft clay: case study. *Journal of Geotechnical and Geoenvironmental Engineering*, 133(12):1483-1493. https://doi.org/10.1061/(ASCE)1090-0241(2007)133:12(1483)

Liu HL, Kong GQ, Chu J, et al., 2015. Grouted gravel column-supported highway embankment over soft clay: case study. *Canadian Geotechnical Journal*, 52(11):1725-1733. https://doi.org/10.1139/cgj-2014-0284

Low BK, Tang SK, Choa V, 1994. Arching in piled embankments. *Journal of Geotechnical Engineering*, 120(11):1917-1938. https://doi.org/10.1061/(ASCE)0733-9410(1994)120:11(1917)

Lu W, Miao L, Wang F, et al., 2020. A case study on geogrid-reinforced and pile-supported widened highway embankment. *Geosynthetics International*, 27(3):261-274. https://doi.org/10.1680/jgein.19.00024

Marston A, Anderson AO, 1913. The Theory of Loads on Pipes in Ditches and Tests of Cement and Clay Drain Tile and Sewer Pipe. Iowa Engineering Experiment Station Bulletin No. 31, Iowa Engineering Station, Iowa State College of Agriculture and Mechanic Arts, Ames, IA, USA.

McKelvey JA, 1994. The anatomy of soil arching. *Geotextiles and Geomembranes*, 13(5):317-329. https://doi.org/10.1016/0266-1144(94)90026-4

Nguyen VD, Luo Q, Wang TF, et al., 2023. Load transfer in geosynthetic-reinforced piled embankments with a triangular arrangement of piles. *Journal of Geotechnical and Geoenvironmental Engineering*, 149(2):04022131. https://doi.org/10.1061/JGGEFK.GTENG-10586

Nunez MA, Briançon L, Dias D, 2013. Analyses of a pile-supported embankment over soft clay: full-scale experiment, analytical and numerical approaches. *Engineering Geology*, 153:53-67. https://doi.org/10.1016/j.enggeo.2012.11.006

Pham TA, 2019. Analysis of soil-foundation-structure interaction to load transfer mechanism in reinforced piled embankments. *Australian Geomechanics Journal*, 54(1):85-100.

Pham TA, 2020. Load-deformation of piled embankments considering geosynthetic membrane effect and interface friction. *Geosynthetics International*, 27(3):275-300. https://doi.org/10.1680/jgein.19.00030

Pham TA, Dias D, 2021a. 3D numerical study of the performance of geosynthetic-reinforced and pile-supported embankments. *Soils and Foundations*, 61(5):1319-1342. https://doi.org/10.1016/j.sandf.2021.07.002

Pham TA, Dias D, 2021b. Comparison and evaluation of analytical models for the design of geosynthetic-reinforced and pile-supported embankments. *Geotextiles and Geomembranes*, 49(3):528-549. https://doi.org/10.1016/j.geotexmem.2020.11.001

Pham TA, Dias D, 2022. A simplified model for the analysis of piled embankments considering arching and subsoil consolidation. *Geotextiles and Geomembranes*, 50(3):408-431. https://doi.org/10.1016/j.geotexmem.2021.12.003

Pham TA, Wijesuriya K, Dias D, 2022. Analytical model for the design of piled embankments considering cohesive soils. *Geosynthetics International*, 29(4):369-388. https://doi.org/10.1680/jgein.21.00034

Rogbeck Y, Alén C, Franzén G, et al., 2003. Nordic Guidelines for Reinforced Soils and Fills. Nordic Geosynthetic Group, Linköping, Sweden.

Rui R, Han J, van Eekelen SJM, et al., 2019. Experimental investigation of soil-arching development in unreinforced and geosynthetic-reinforced pile-supported embankments. *Journal of Geotechnical and Geoenvironmental Engineering*, 145(1):04018103. https://doi.org/10.1061/(ASCE)GT.1943-5606.0002000

Smith EJ, Bouazza A, King LE, 2022. Numerical simulation of the progressive development of soil arching in column-supported embankments. *Canadian Geotechnical Journal*, 59(2):159-176. https://doi.org/10.1139/cgj-2020-0672

Sun YH, Wang HL, Meng FY, et al., 2025. Multiscale mechanical behaviour of sand-steel structure interface for deep underground space. *Canadian Geotechnical Journal*, 62:1-16. https://doi.org/10.1139/cgj-2025-0026

Terzaghi K, 1943. Theoretical Soil Mechanics. John Wiley & Sons, New York, USA. https://doi.org/10.1002/9780470172766

Terzaghi K, Peck RB, Mesri G, 1996. Soil Mechanics in Engineering Practice. 3rd Edition. John Wiley & Sons, New York, USA.

van Eekelen SJM, Brugman MHA, 2016. Design Guideline Basal Reinforced Piled Embankments. CRC Press, Boca Raton, Florida, USA.

van Eekelen SJM, Han J, 2020. Geosynthetic-reinforced pile-supported embankments: state of the art. *Geosynthetics International*, 27(2):112-141. https://doi.org/10.1680/jgein.20.00005

van Eekelen SJM, Bezuijen A, Oung O, 2003. Arching in piled embankments; experiments and design calculations. Proceedings of the International Conference on Foundations, p.885-894.

van Eekelen SJM, Bezuijen A, Alexiew D, 2008. Piled embankments in the Netherlands, a full-scale test, comparing 2 years of measurements with design calculations. Proceedings of the 4th European Geosynthetics Conference, p.264.

van Eekelen SJM, Bezuijen A, Alexiew D, 2010. The Kyoto road piled embankment: 3½ years of measurements. Proceedings of the 9th International Conference on Geosynthetics, p.1941-1944.

van Eekelen SJM, Bezuijen A, Lodder HJ, et al., 2012. Model experiments on piled embankments. Part I. *Geotextiles and Geomembranes*, 32:69-81. https://doi.org/10.1016/j.geotexmem.2011.11.002

van Eekelen SJM, Bezuijen A, van Tol AF, 2013. An analytical model for arching in piled embankments. *Geotextiles and Geomembranes*, 39:78-102. https://doi.org/10.1016/j.geotexmem.2013.07.005

van Eekelen SJM, Bezuijen A, van Tol AF, 2015. Validation of analytical models for the design of basal reinforced piled embankments. *Geotextiles and Geomembranes*, 43(1):56-81. https://doi.org/10.1016/j.geotexmem.2014.10.002

van Eekelen SJM, Venmans AAM, Bezuijen A, et al., 2020. Long term measurements in the Woerden geosynthetic-reinforced pile-supported embankment. *Geosynthetics International*, 27(2):142-156. https://doi.org/10.1680/jgein.17.00022

Wang HL, Chen RP, 2019. Estimating static and dynamic stresses in geosynthetic-reinforced pile-supported track-bed under train moving loads. *Journal of Geotechnical and Geoenvironmental Engineering*, 145(7):04019029. https://doi.org/10.1061/(ASCE)GT.1943-5606.0002056

Wang HL, Yin ZY, 2020. High performance prediction of soil compaction parameters using multi expression programming. *Engineering Geology*, 276:105758. https://doi.org/10.1016/j.enggeo.2020.105758

Wang HL, Chen RP, Qi S, et al., 2018. Long-term performance of pile-supported ballastless track-bed at various water levels. *Journal of Geotechnical and Geoenvironmental Engineering*, 144(6):04018035. https://doi.org/10.1061/(ASCE)GT.1943-5606.0001890

Wang HL, Chen RP, Cheng W, et al., 2019a. Full-scale model study on variations of soil stress in geosynthetic-reinforced pile-supported track bed with water level change and cyclic loading. *Canadian Geotechnical Journal*, 56(1):60-68. https://doi.org/10.1139/cgj-2017-0689

Wang HL, Chen RP, Liu QW, et al., 2019b. Investigation on geogrid reinforcement and pile efficacy in geosynthetic-reinforced pile-supported track-bed. *Geotextiles and Geomembranes*, 47(6):755-766. https://doi.org/10.1016/j.geotexmem.2019.103489

Wang HL, Yin CS, Zhang QY, et al., 2024. Monotonic mechanical behaviour of compacted completely decomposed granite with various inclusion levels of incineration bottom ash. *Journal of Zhejiang University-SCIENCE A*, 25(8):670-679. https://doi.org/10.1631/jzus.A2300514

Xing HF, Zhang Z, Liu HB, et al., 2014. Large-scale tests of pile-supported earth platform with and without geogrid. *Geotextiles and Geomembranes*, 42(6):586-598. https://doi.org/10.1016/j.geotexmem.2014.10.005

Xu C, Song S, Han J, 2016. Scaled model tests on influence factors of full geosynthetic-reinforced pile-supported embankments. *Geosynthetics International*, 23(2):140-153. https://doi.org/10.1680/jgein.15.00038

Ye GB, Wang M, Zhang Z, et al., 2020. Geosynthetic-reinforced pile-supported embankments with caps in a triangular pattern over soft clay. *Geotextiles and Geomembranes*, 48(1):52-61. https://doi.org/10.1016/j.geotexmem.2019.103504

Ye YQ, Al-Naddaf M, Han J, et al., 2024. Spring-based trapdoor tests evaluating pile-supported load transfer platforms with different fill materials. *Journal of Geotechnical and Geoenvironmental Engineering*, 150(12):04024122. https://doi.org/10.1061/JGGEFK.GTENG-12595

Zaeske D, 2001. Zur Wirkungsweise von Unbewehrten und Bewehrten Mineralischen Tragschichten Über Pfahlartigen Gründungselementen. PhD Thesis, Universität Kassel, Kassel, Germany (in German).

Zhang L, Zhou S, Zhao H, et al., 2018. Performance of geosynthetic-reinforced and pile-supported embankment with consideration of soil arching. *Journal of Engineering Mechanics*, 144(12):06018005. https://doi.org/10.1061/(ASCE)EM.1943-7889.0001536

Zhang XD, Zhuang Y, Hu SL, et al., 2022. A simplified method for assessing the serviceability performance of geosynthetic reinforced and pile-supported embankment. *Geotextiles and Geomembranes*, 50(6):1214-1229. https://doi.org/10.1016/j.geotexmem.2022.08.006

Zhang XH, Wang HL, Fu XS, et al., 2026. Effects of water content and dry density on the passive soil arching effect in unsaturated compacted clay. *Canadian Geotechnical Journal*, in press. https://doi.org/10.1139/cgj-2025-0925

Zhang XH, Zhai ZJ, Wang HL, et al., 2025. A deformation-dependent model for passive soil arching in sand. *Acta Geotechnica* 20:6495-6513. https://doi.org/10.1007/s11440-025-02733-5

Zhao MX, Liu CY, El-Korchi T, et al., 2019. Performance of geogrid-reinforced and PTC pile-supported embankment in a highway widening project over soft soils. *Journal of Geotechnical and Geoenvironmental Engineering*, 145(11): 06019014. https://doi.org/10.1061/(ASCE)GT.1943-5606.0002157

Zhou YL, Wang X, He F, et al., 2023. Calculation method and model tests of pile frost jacking for railway overhead contact systems in permafrost regions. *Cold Regions Science and Technology*, 206:103746. https://doi.org/10.1016/j.coldregions.2022.103746

Zhuang Y, Wang KY, 2016. Finite-element analysis on the effect of subsoil in reinforced piled embankments and comparison with theoretical method predictions. *International Journal of Geomechanics*, 16(5):04016011. https://doi.org/10.1061/(ASCE)GM.1943-5622.0000628

Zhuang Y, Ellis E, Yu HS, 2012. Three-dimensional finite-element analysis of arching in a piled embankment. *Géotechnique*, 62(12):1127-1131. https://doi.org/10.1680/geot.9.p.113

Zhuang Y, Wang KY, Liu HL, 2014. A simplified model to analyze the reinforced piled embankments. *Geotextiles and Geomembranes*, 42(2):154-165. https://doi.org/10.1016/j.geotexmem.2014.01.002

Electronic supplementary materials

Sections S1–S5, Tables S1–S5, Figs. S1–S2